Biomaterials Science

Design of Biomaterials for intracellular delivery of carbon monoxide

Journal:	*Biomaterials Science*
Manuscript ID:	BM-MRV-06-2015-000210.R1
Article Type:	Minireview
Date Submitted by the Author:	23-Jul-2015
Complete List of Authors:	Inaba, Hiroshi; Kyoto University, Department of Synthetic Chemistry and Biological Chemistry Fujita, Kenta; Tokyo Institute of technology, Ueno, Takafumi; Tokyo Institute of Technology, Department of Biomolecular Engineering

SCHOLARONE™
Manuscripts

Design of Biomaterials for intracellular delivery of carbon monoxide

Hiroshi Inaba,[a] Kenta Fujita[b] and Takafumi Ueno*[b]

[a]Department of Chemistry, Roger Adams Laboratory, University of Illinois, 600 South Mathews, Urbana, Illinois 61801, United States.

[b]Department of Biomolecular Engineering, Graduate School of Bioscience and Biotechnology, Tokyo Institute of Technology, Nagatsuta-cho, Midori-ku, Yokohama 226-8501, Japan. E-mail: tueno@bio.titech.ac.jp

Abstract

Carbon monoxide (CO) is recognized as one of the most important gas signaling molecules involved in governing various therapeutic responses. Intracellular generation of CO is spatiotemporally controlled by catalytic reactions of heme oxygenases (HOs). Thus, the ability to control intracellular CO delivery with modulation of the CO-release rate in specific amounts and locations is expected to improve our fundamental understanding of the functions of CO and development of clinical applications. For this purpose, CO-releasing molecules (CORMs) have been developed and investigated *in vitro* and *in vivo*. Most CORMs are based on transition metal carbonyl complexes. Recently, various biomaterials consisting of metal carbonyls with biomacromolecular scaffolds have been reported to improve the properties of bare metal carbonyls. In this mini-review, current progress in CO delivery, recent strategies for development of CORMs, and future directions of this field are discussed.

1. Introduction

A number of gaseous molecules including dioxygen (O_2), nitric oxide (NO), hydrogen sulfide (H_2S), and carbon monoxide (CO) cooperatively play unique roles as messengers of cellular signal transduction.[1-3] Compared to O_2, NO, and H_2S, CO is stable and predominantly binds to transition metals, especially reduced iron centers of metalloproteins. In particular, CO binds to hemoproteins to modulate cellular functions including redox control, gene regulation, and enzymatic reactions.[4,5] Because intracellular CO is involved in several selective reactions, design of biomaterials that can deliver CO into cells is an attractive approach in efforts to modulate cellular functions.[1,6-8] The existence of CO in human blood was identified in the 19th century. It has been reported that CO is generated by the heme degradation reaction catalyzed by heme oxygenase (HO) at a rate of approximately 20 $\mu mol \cdot h^{-1}$ in the human body.[9] HO produces CO, iron(II) ion, and biliverdin and each of these molecules plays a role in cellular signaling.[10,11] There are three isozymes of HO, which are designated HO-1, HO-2, and HO-3.[10,11] These isozymes vary in terms of localization, expression levels, and the functions. HO-1, which is induced in response to stress, is highly expressed in spleen, liver, and bone marrow.[10,11] HO-2 and HO-3 both exhibit constitutive activity in essentially all tissues. The HO isozymes are thought to modulate neurotransmission because of their distribution in the brain. Moreover, the three isozymes of HO are genetically distinct as confirmed by previous biological experiments. HO-1 is a stress protein (32 kDa) whose coding genes effect a transcriptional response to protect cell from stress.[10,11] In terms of the reactivity of the heme degradation, HO-1 has a K_m value of 0.24 μM which is one-third lower than that of HO-2 (0.67 μM).[11] The rate of

bilirubin production promoted by HO-1 (3.4 μmol/mg of protein/h) is 14-fold higher than that of HO-2 (0.24 μmol/mg of protein/h).[12] The quick response of HO-1 is consistent with its reported activity in protecting cells from stress. HO-3 has ~90% amino acid homology with HO-2 and these two isozymes both include putative heme regulatory domains.[10,11] Subcellular localization is also an important feature of the HOs. HO-1 is localized in the endoplasmic reticulum, mitochondria, nucleus, and plasma membrane.[10,11,13] External stimuli such as lipopolysaccharide and heme dramatically affect both expression levels and localization of HO-1.[14] The subcellular compartmentalization of HO-1 strongly suggests that localized HO metabolites, such as CO, have specific functions in these organelles. The tight regulation of generation of CO in a spatiotemporal manner indicates that delivery of CO with specific localization and timing is a promising strategy for modulating natural signaling processes. Knockdown and overexpression of HO-1 are useful strategies to study the effects of HO-1 on the cellular signaling.[10,11] However, the localization, amount, and rates of CO generation are difficult to control. The capability to provide an exogenous CO source that can deliver CO in a spatiotemporal manner would enable us to obtain information about the role of CO in signaling pathways.

Inhalation of CO gas is the simplest mode of CO delivery and has been applied in clinical trials.[5] However, the diffusion of CO gas prevents localized delivery. In addition, CO gas tends to induce cytotoxicity by binding to hemoglobin. Thus, various strategies have been developed by chemists to construct molecular scaffolds known as CO-releasing molecules (CORMs) to provide vehicles for intracellular CO delivery.[1,6-8] Most CORMs are based on metal carbonyls, and the first- and second-coordination spheres can be modified to confer appropriate properties. For example, the kinetics of

CO release can be altered. In addition, various types of biomaterials have recently been used as carriers of CORMs. Biomaterial-based CORMs with improved properties are attractive candidates for providing intracellular CO delivery in a spatiotemporal manner (Fig. 1). In this mini-review, we provide an overview of progress in the rational design and development of CORMs with a particular focus on the use of biomacromolecular scaffolds.
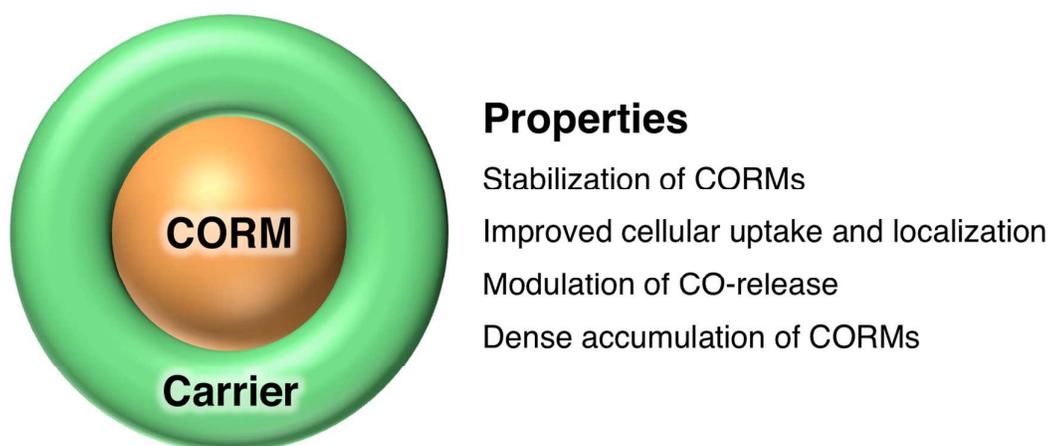

Properties

Stabilization of CORMs

Improved cellular uptake and localization

Modulation of CO-release

Dense accumulation of CORMs

Fig. 1. Incorporation of CORM in macromolecular carrier for intracellular CO delivery.

2. Carbon monoxide-releasing molecules (CORMs)

The first CORMs were reported by Motterlini and co-workers.[15] Several metal carbonyls, $Fe(CO)_5$, $Mn_2(CO)_{10}$ (CORM-1), and $[Ru(CO)_3Cl_2]_2$ (CORM-2) were demonstrated to release CO under physiological conditions. $Fe(CO)_5$ and CORM-1 release CO in response to light and CORM-2 releases CO in ligand-exchange reactions. CORM-2 has been shown to induce vasodilatation and hypotension *in vivo*.[15] To improve the water solubility of CORM-2, $Ru(CO)_3Cl(glycinate)$ (CORM-3) has been

developed.[16] CORM-3 exerts a cardioprotective effect *in vitro* and *in vivo*.[16] Based on these important findings, CORM-2 and CORM-3 have been well characterized and are the most frequently-used CORMs in investigations of the physiological functions of CO *in vitro* and *in vivo* (Fig. 2). CORM-2 and CORM-3 are expected to release CO by interaction with intracellular anions such as thiol-containing molecules.[17,18] The CORMs are unstable under most physiological conditions in terms of half-life ($t_{1/2}$). For example, the half-life of CORM-3 in human plasma is 3.6 min.[19] The ability to provide rapid release of CO may be beneficial to induce a prompt cellular response against CO. By using CORM-2 and CORM-3, various functions of CO have been clarified, including anti-inflammatory, anti-ischemic, anti-apoptotic, and vasodilatory effects through pathways that include p38, mitogen activated protein kinases (MAPKs), and nuclear factor-kappaB (NF-κB), among others.[20] However, endogenous CO is locally generated by HOs and temporal control of CO release is required to study the physiological functions of CO and investigate them in *in vivo* applications.[7] In addition, CO release from CORM-2 and CORM-3 yields Ru-containing moieties that may induce unexpected effects such as cytotoxicity.[7] To overcome such issues, a wide variety of transition metals and ligands have been investigated. Stimulus-induced CO release is a promising strategy to perform controlled CO delivery into cells. In this section, CO-releasing properties of CORMs induced by light and other stimuli (enzymes, pH and temperature) are described.
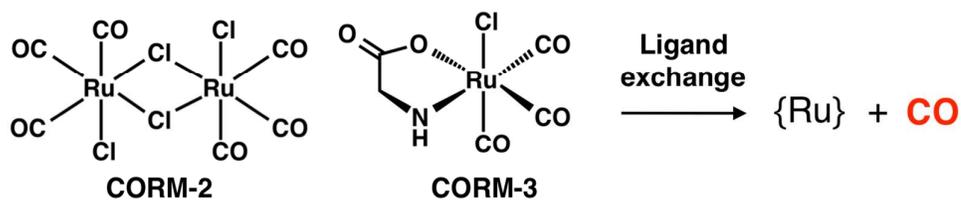
Fig. 2. CORMs that have been most frequently utilized for *in vitro* and *in vivo* applications.

2-1.   Photo-activated CORMs (photoCORMs)

Since the first photoCORMs $Fe(CO)_5$ and $Mn_2(CO)_{10}$ (CORM-1) were reported,[15] various photoactivated CORMs have been developed and described in a number of reviews.[21-24] Most photoCORMs are transition metal complexes of Fe,[25-27] Mn,[28-35] Ru,[36] Re,[31,37] Mo,[38] and W.[39] Notable examples are shown in Fig. 3a. An iron-based CORM with biogenic ligands known as CORM-S1 releases CO upon irradiation with visible light ($\lambda > 400$ nm).[25] The light-induced CO release was confirmed to activate voltage- and Ca^{2+}-activated potassium channels.[25] A manganese-based CORM with tripodal polypyridine ligands, $[Mn(pqa)(CO)_3]^+$ releases CO upon irradiation with UV (305 nm) or visible ($\lambda > 350$ nm) light.[34] The apparent CO release rate k_{CO} value of the manganese carbonyls is higher with UV irradiation ((8.1 ± 0.2) $\times$ 10^{-2} s^{-1}) than with visible light irradiation ((8.3 ± 0.2) $\times$ 10^{-3} s^{-1}). $[Mn(pqa)(CO)_3]^+$ is stable in aqueous solution and induces vasorelaxation in mouse aortic muscle rings upon irradiation with visible light. A rhenium-based CORM, $[Re(bpy)(CO)_3(L)]^+$ releases CO after photolysis induced by irradiation with 405 nm light.[37] Notably, since both $[Re(bpy)(CO)_3(L)]^+$ and the rhenium complex after CO release are luminescent, CO release in cells can be tracked using confocal fluorescence

microscopy. Since the transition metals may induce cytotoxicity after CO release, organic photoCORMs have recently been developed.[40] A fluorescein analogue, 6-hydroxy-3-oxo-3*H*-xanthene-9-carboxylic acid has been shown to release CO upon irradiation with 500 nm light (Fig. 3b).[40] The compound undergoes photo-induced CO release at pH 5.7-7.4. The improved properties of the photoCORMs including water solubility, spectroscopic properties, and reduced toxicity of photoproducts after CO release demonstrates their potential for use in biological and clinical applications. Theoretical studies have indicated that photoCORMs can be structurally designed to promote photo release of CO at desired wavelengths.[32,41] The design is based on transitions of metal-to-ligand charge transfer (MLCT) of metal carbonyls, which contribute to stability of metal-CO bond and CO release. Density functional theory (DFT) and time-dependent DFT (TDDFT) calculations were performed on the Mn(I) carbonyl complexes (**1-4**) in investigations aimed at understanding the effects of the ligands on the transitions of HOMO-2 to LUMO (Fig. 4).[32,41] The calculations demonstrated that the smaller energy difference between HOMO-2 and LUMO in **2** relative to **1** causes a red shift of the MLCT band. The ancillary ligands also have an effect on the energy difference, as the σ-donating Br^- ligand in **2** raises the HOMO-2 level relative to the CH_3CN ligand in **3**, resulting in a red shift of the transition from the HOMO-2 to LUMO. In a comparison of **3** and **4**, the SCH_3 group of qmtpm is shown to have an effect on the slight increase of the HOMO-2 level to induce a red shift. These results indicate that the ligands strongly influence the MLCT of the metal complexes. Based on these design principles, optimization of the chemical structures is expected to expand the possibility of developing photoCORMs for applications *in vitro* and *in vivo*. In particular, initiating CO release by irradiation with near-infrared (NIR) window light

(650-900 nm) is expected to be available for *in vivo* applications because the light can penetrate biological tissues more effectively than visible light.[42] In another approach, incorporation of photoCORMs into macromolecular scaffolds provides the ability to tune the photochemical properties as described in Section 3.
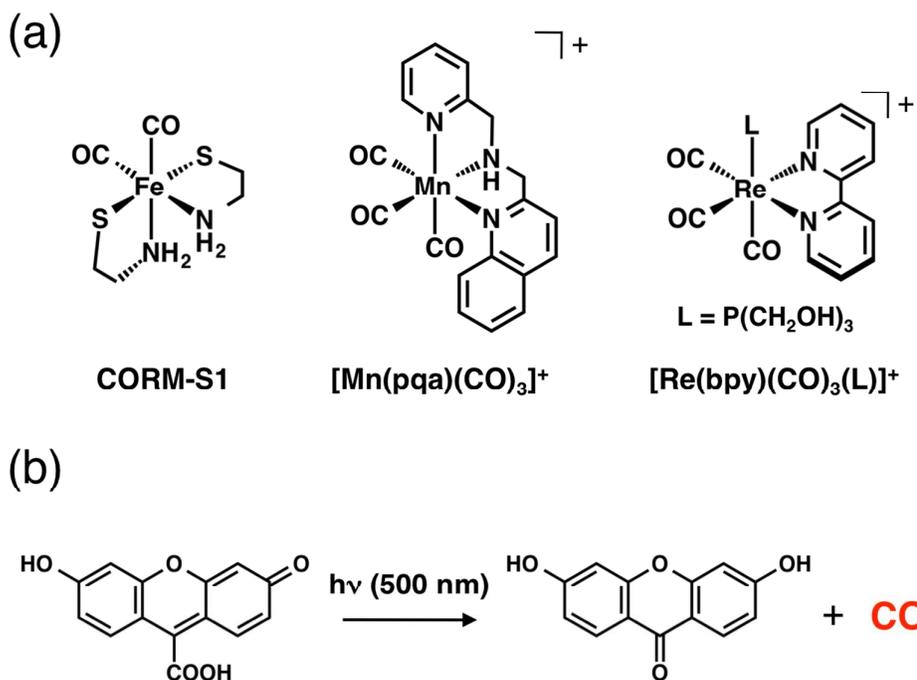
(a)

CORM-S1   [Mn(pqa)(CO)₃]⁺   [Re(bpy)(CO)₃(L)]⁺

(b)

Fig. 3. Selected photoCORMs based on (a) metal carbonyls[25,34,37] and (b) an organic molecule.[40]
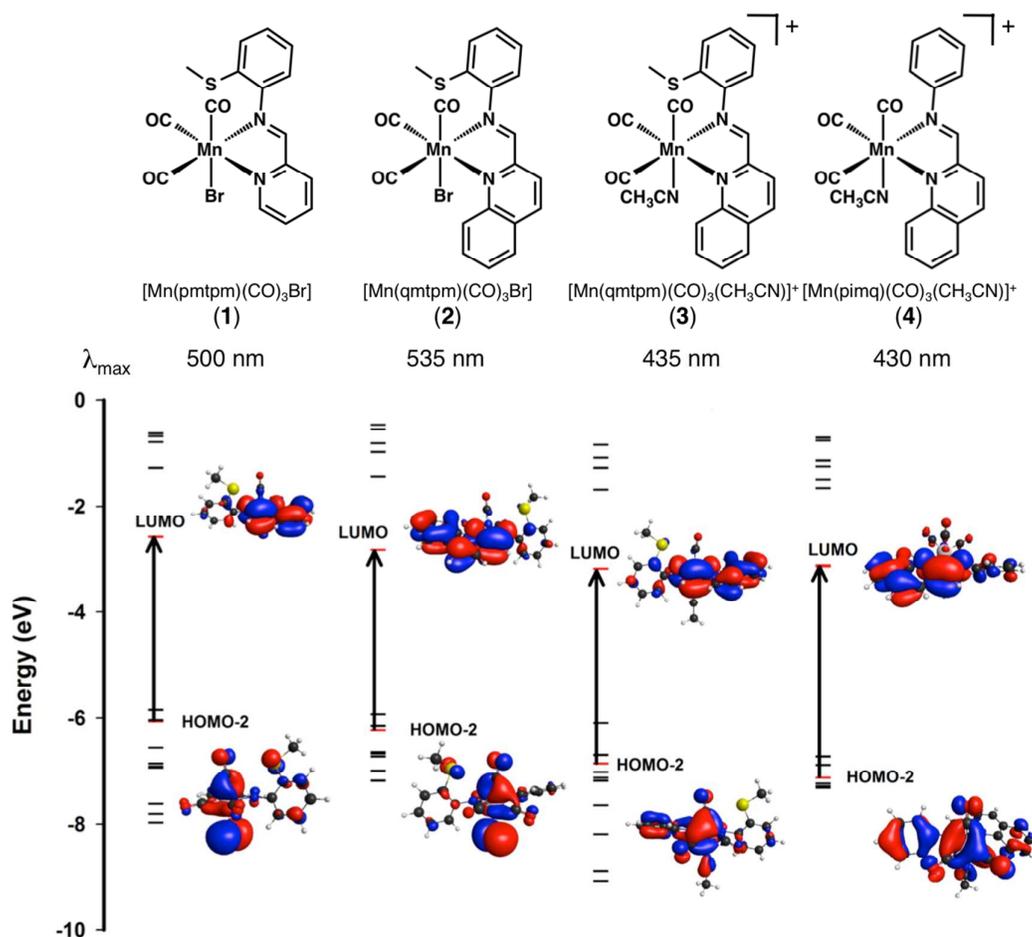
Fig. 4. Calculated HOMO/LUMO energy diagram of complexes 1-4.[41] The most prominent MOs involved with transitions under the low-energy band and their diagrams are shown. Modified from ref. 41 with permission from American Chemical Society.

2-2.   CORMs activated by other stimuli

Na$_2$(H$_3$B-CO$_2$) (CORM-A1) is the first non-transition metal-containing CORM that provides pH- and temperature-dependent CO release (Fig. 5a).[43,44] Under acidic conditions, first and second protonations occur and then subsequent water cleavage forms the highly unstable H$_3$B-CO complex. Since the formation of H$_3$B-CO is the

rate-limiting step, as pH decreases, the concentration of the double-protonated CORM-A1 increases to accelerate the rate of CO release. The half-life of CO release from CORM-A1 at 37°C is 21 minutes at pH 7.4 and 2.0 minutes at pH 5.5. By substituting the carboxylate of CORM-A1 to amides, the CO release rate is decelerated.[45] The slow rate of CO release is due to the higher pK_a values of amides relative to carboxylates. The different CO release rates of CORM-A1 and CORM-3 influence the vasorelaxation effect. CORM-A1 promotes gradual and sustained vasorelaxation whereas CORM-3 has an immediate effect, indicating the importance of the CO release rate.

Schmalz and co-workers have developed enzyme-triggered CORMs (ET-CORMs).[46-52] This concept is based on enzymatic reactions of intracellular enzymes with ligands of CORMs designed as esterase-reactive moieties. The first examples of ET-CORMs were acyloxybutadiene–Fe(CO)$_3$ complexes.[46] After cell entry, the ester group of the complex is cleaved in a reaction catalyzed by intracellular esterases. The resulting dienol–Fe(CO)$_3$ complexes readily decompose under mild oxidation conditions and release three CO molecules (Fig. 5b). Several versions of ET-CORMs have been reported with alterations provided by modifying the substitution pattern[47] and racemic structures,[48] to tune the kinetics of the CO-release reaction and the amounts of CO released (Fig. 5c). As shown in Fig. 5b, the CO-release rates from the ET-CORMs are dependent on the rate of ester hydrolysis and the stability of the enol intermediates. Complex **5** releases CO faster than complex **6**, presumably due to the faster enzymatic cleavage (Fig. 5c).[48] A phosphoryloxy–Fe(CO)$_3$ complex (**7**) has been reported as a water-soluble and phosphatase reactive CORM.[49] The effects of these ET-CORMs have been investigated by evaluating their influence on cell viability and

activity of inducible NO synthase (iNOS). One of the drawbacks of ET-CORMs is generation of byproducts including enones and Fe^{3+} ions, which may induce cellular signaling and/or cytotoxicity. The authors have synthesized ligand-substituted ET-CORMs and ketones to evaluate their effects on iNOS-inhibition activity and cytotoxicity (Fig. 5d).[47] The π-ligand and the nature of the acyloxy substituent strongly affects the CO-release rate, the inhibition of iNOS activity, and the cytotoxicity of the ET-CORMs (Fig. 5d).[47] It has been shown that (1) introduction of bulky ester units to an acetate core-structure reduces NO-inhibition activity and cytotoxicity; (2) diesters have increased NO-inhibition activity and cytotoxicity; and (3) geminal dimethylation at the cyclohexadiene scaffold reduces cytotoxicity with a slight decrease of NO-inhibition activity. Development of protease-triggered CORMs has also been recently reported.[50] The CORMs consist of a peptidase-specific oligopeptide, a self-immolative linker, and an oxycyclohexadiene–$Fe(CO)_3$ (Fig. 5e). By enzymatic cleavage of the specific oligopeptide, the linker is eliminated from the complex to generate a dienol–$Fe(CO)_3$ unit, resulting in CO release under oxidative conditions. Penicillin G amidase (PGA)-cleavable phenylacetamide was used as a model of protease specificity. The CORMs were found to inhibit the inflammatory response and induce expression of HO-1 in human endothelial cells only upon addition of both the CORM and PGA, indicating that the amidase-induced cleavage reaction occurs in these cells. These reports show that ET-CORMs with specifically-designed chemical structures are attractive candidates for providing controlled CO release in cellular environments. Further development focusing on enzymatic specificity will open a new direction for providing selective CO release in specific cells and subcellular compartments.

Fig. 5. (a) CORM-A1 and derivative.[43-45] (b) Enzyme-triggered (ET)-CORMs.[46] (c) Derivatives of ET-CORMs.[48,49] (d) Design of ET-CORMs.[47] (e) Protease-triggered ET-CORMs.[50] Modified from ref 47 and 50 with permission from the Royal Society

of Chemistry and Wiley-VCH, respectively.

3. Molecular scaffold-incorporated CORMs

As described in the previous section, various ligands have been developed to construct CORMs with desired properties such as improved water solubility, stimuli-responsive CO release and reduced cytotoxicity. However, small molecules have several drawbacks including random diffusion, toxicity derived from metal ions, and low cellular uptake efficiency, which may prevent their use in biological studies. In particular, the design of ligands for cellular uptake is a truly challenging task because CORMs should be sufficiently lipophilic to pass through the cellular membrane, but excess lipophilicity may induce accumulation of CORMs within the cell membrane. It is difficult to control localization of CORMs in specific organelles. As described in recent reviews,[7,8] incorporation of CORMs into macromolecular carriers is a powerful method for improving the properties of bare CORMs. Potential advantages of this strategy are (1) stabilization of the CORMs and metal complexes after CO release; (2) improvement of cellular uptake and intracellular localization; (3) modulation of CO-releasing amounts and rates; and (4) dense accumulation of CORMs within carriers (Fig. 1). Recently, CORMs conjugated to various macromolecular carriers have been reported. We categorize the carriers as synthetic polymers (micelles, nanoparticles, dendrimers, copolymers, fibers, and metal organic frameworks (MOFs)) and biomolecules (peptides, vitamins, monomeric proteins, and self-assembled supramolecular proteins) in Table 1. In this section, we describe the design strategy of the newest classes of CORMs.

14

Table 1. CORMs conjugated with macromolecular carriers.

	Constituent molecules	CORM moieties and methods	Size	CO release (Amount) (Rate) (Mechanism)	Biological assay	Properties	Ref
Micelles	PEG block and poly(*n*-butylacryl-amide) block	CORM-3 Chemical modification	29 - 44 nm	0.76 equiv. of CO / Ru Slower than CORM-3 Spontaneous	Attenuation of LPS-induced NF-κB activation in human monocytes	Inhibition of diffusion of CO release trigger	18
	Styrene-maleic acid copolymer	CORM-2 Non-covalent incorporation	165.3 ± 71 nm	Not calculated Slower than CORM-2 Ligand exchange	Suppression of up-regulated inflammatory cytokines in mice	Inhibition of degradation of CORM-2 in aqueous media	53
	Block copolymers of polyethylene oxide and polypropylene oxide	Unsaturated cyclic α-diketones (DKs) Non-covalent incorporation	–	84% of CO / DKs Not calculated 470 nm light	No cytotoxicity in KG-1 cells	Inhibition of diffusion of DKs in living cells	54
Nanoparticles	Fe_2O_3	CORM-3 Chemical modification	9 ± 2 nm	Not calculated $t_{1/2} = 7 ± 2$ min Magnetic field	–	Magnetic filed-induced CO release	55
	SiO_2	$[Mn(CO)_3(tpm)]^+$ Chemical modification	20 nm	Not calculated Not calculated 365 nm light	–	Target delivery of CORMs	56
	Nanodiamond	$[Mn(CO)_3(tpm)]^+$ Chemical modification	10 nm	Not calculated Not calculated 365 nm light	–	Target delivery of CORMs	57
	Tm and Yb-doped $NaGdF_4$ UCNP	$[Mn(bpy)(CO)_2(PPh_3)_2]^+$ Non-covalent incorporation	16-30 nm	Not calculated Not calculated 980 nm NIR	–	NIR-induced CO release	58
Dendrimers	Polypyridyl dendrimers	$[MnBr(bpy)(CO)_3]$ Chemical modification	–	1.5-15.2 equiv. of CO / composites (dependent on the molecular weight) $t_{1/2} = 7.4$-16.8 min (dependent on the molecular weight) 410 nm light	–	Delivery of large amounts of CORMs	59

Copolymers	HPMA	[(bpma)Mn(CO)₃]⁺ Chemical modification	–	Not calculated $t_{1/2}$ = 20 min 365 nm light	Size and molecular weight-depended toxic effects in HepG2 cells	Target accumulation of CORMs	60
Mesoporous silica nanoparticles	Al-MCM-41	[Mn(pqa)(CO)₃]ClO₄ Non-covalent incorporation	58.9 ± 7.7 nm	Not calculated Not calculated > 350 nm light	Induction of relaxation of rat aorta muscle rings in tissue bath experiments	Target accumulation of CORMs	61
Fibers	Poly(L-lactide-*co* -D/L-lactide) (70:30)	CORM-1 Non-covalent incorporation	1 μm (diameter)	3.4 ± 0.3 μmol CO per mg of fiber $t_{1/2}$ = 309 and 1281 sec (dependent on the wavelength of light) 365-480 nm light	Photo-induced cytotoxicity mouse fibroblast 3T3 cells	High surface area for tuning molecular release profiles	62
MOFs	MIL-88B-Fe	CO gas Non-covalent incorporation	2.4 × 1.2 μm (spindle shape)	0.36 μmol / mg of MOFs $t_{1/2}$ = 38 min Degradation	–	Stable absorption of CO gas	63
Peptides	Thr-Phe-Ser-Asp-Leu	[Mn(CO)₃(tpm)]PF₆ Chemical modification	–	1.7 equiv. of CO / Mn Not calculated 365 nm light	–	Target delivery of CORMs	64
	Leu-Pro-Leu-Gly -Asn-Ser-His	[Mo(CO)₄(bpy^CH3,CHO)] Chemical modification	–	2.4 ± 0.4 equiv. of CO / Mo $t_{1/2}$ = 44 ± 7 min 468 nm light	–	Target delivery of CORMs	65
	Leu-Pro-Leu-Gly -Asn-Ser-His	[Mn(bpea^CH2C6H4CHO)- (CO)₃]PF₆ Chemical modification	–	1.70 ± 0.08 equiv. of CO / Mn $t_{1/2}$ = 15.51 ± 0.52 min 365 nm light	–	Target delivery of CORMs	66
	C₁₆-(Val)₃-(Ala)₃ -(Glu)₃-Lys	CORM-3 Chemical modification	–	Not calculated $t_{1/2}$ = 2.16 ± 0.05 min Spontaneous	Cardioprotective effect on oxidatively stressed H9c2 rat cardiomyocytes	Target accumulation of CORMs	67
	Ala-Glu	[Fe(CO)(N4Py)]²⁺ Chemical modification	–	Not calculated Not calculated Not measured	–	Target delivery of CORMs	27
	PNA	[RuCl₂(bpy)(CO)₂] Chemical modification	–	0.3 ± 0.1 equiv. of CO / Ru $t_{1/2}$ = 24 ± 10 min 365 nm light	–	Target delivery of CORMs	36

Vitamins	B_{12}	$[Re(CO)_2Br_2]$ Chemical modification	–	1.0 equiv. of CO / Re $t_{1/2}$ = 20-30 min Spontaneous	No uptake into neonatal rat cardiomyocytes	Transcobalamin transporter-targeted delivery of CORMs	68
	B_{12}	$[(tacd)Mn(CO)_3]^+$ Chemical modification	–	3.0 equiv. of CO / Mn Not calculated 470 nm light	Cytoprotective effects to 3T3 fibroblasts against hypoxia and metabolic depletion	Transcobalamin transporter-targeted delivery of CORMs	69
	Galactose	CORM-2 Chemical modification	–	1 equiv. of CO / Ru Not calculated Spontaneous	Protection of mice from experimental cerebral malaria	Liver-targeted delivery of CORMs	70
	2-isocyano-2-methyl-propanoate	$Mo(CO)_3$ Chemical modification	–	1.2 equiv. of CO / Mo Not calculated Spontaneous	Reduction of an acetaminophen-induced severe acute liver injury	Liver-targeted delivery of CORMs	71
	Hybrid	$[Co_2(CO)_6]$ Chemical modification	–	1.3 equiv. of CO / Co $t_{1/2}$ = 21 min Spontaneous	Nuclear accumulation of Nrf2 and HO-1 expression in murine microglial BV2 cells and murine RAW 264.7 macrophages	Activation of Nrf2 and release of CO	72
Proteins	BSA	$Ru(CO)_2$ Coordination to amino acid residue	–	Not calculated Not calculated Spontaneous	Down-regulation of an expression levels of TNF-α, IL-6, and IL-10 in HeLa and Caco-2 cells	Safe and spatially controlled delivery of CORMs	73
	IL-8	$Ru(CO)_2$ Coordination to amino acid residue	–	Not calculated Not calculated Spontaneous	Retention of inherent neutrophil chemotaxis of IL-8 in HeLa cells	Safe and spatially controlled delivery of CORMs	74
	Fr	$Ru(CO)_2$ Coordination to amino acid residue	12 nm	0.16 ± 0.04 equiv. of CO / Ru 35.5 ± 0.3 min Spontaneous	NF-κB activation in HEK293 cells	Slow CO release and highly-effective transport	75
	HEWL crystal	$Ru(CO)_2$ Coordination to amino acid residue	2 μm	0.38 ± 0.02 equiv. of CO / Ru 19.4 ± 1.4 min Spontaneous	NF-κB activation in HEK293 cells	Slow CO release in extracellular environment	76
	PhC	$Ru(CO)_2$ Coordination to amino acid residue	–	6.2 ± 0.9 equiv. of CO / monomer 27.7 ± 1.6 min Spontaneous	NF-κB activation in HEK293 cells	Slow CO release in extracellular environment	77

3-1. Synthetic polymer materials

3-1-1. Materials for cellular transport

It is difficult to induce release of CO from most CORMs in cellular environments because they have low solubility and low cellular uptake efficiency.[7,8] To address the issue, development of carrier molecules for transporting CORMs has been considered essential in order to achieve effective transport into living cells. Micelle[18,53,54] and nanoparticle[55-58]-based scaffolds for CO release have been utilized because they have been demonstrated as intracellular carrier molecules for Gd imaging probes[79] and various metal drugs, such as cisplatin.[78]

Micelle compounds consist of both hydrophilic and hydrophobic components, which improve the solubility and stability of metal complexes in living cells.[18,53,54] In an effort to construct micelle-based CORMs, CORM-3 was covalently anchored between a hydrophilic poly(ethylene glycol) (PEG) block and a hydrophobic poly(*n*-butylacrylamide) block (Fig. 6a).[18] The 29-44 nm-sized composites release 0.76 equiv. of CO per Ru in a PBS buffer solution. The encapsulation of CORM-3 within the PEG-based micelles increases the $t_{1/2}$ of CO because diffusion of trigger molecules for CO release, such as cysteine and glutathione, is inhibited in the micelle. The micelle reduces the cytotoxicity of CORM-3 in human monocytes. The PEG micelle attenuates LPS-induced NF-κB activation, while naked CORM-3 has no beneficial effects with respect to activation.

Maeda *et al.* demonstrated encapsulation of CORM-2 with a water-soluble styrene-maleic acid (SMA) copolymer-based micelle with a hydrodynamic size of 165.3 ± 71 nm (Fig. 6b).[53] The release rate of CO of the composite was found to be slower than that of free CORM-2. When mice were treated with the composite, up-regulation

of inflammatory cytokines was significantly suppressed compared to CORM-2 due to suppression of the cytotoxic effect. A block copolymer of polyethylene oxide and polypropylene oxide (Pluronic F127) has been used by Liao and *et al.* to encapsulate unsaturated cyclic α-diketones (DKs) (Fig. 6c).[54] The composite is responsive to 470 nm visible light for release of CO originating from the diketone backbone and it was demonstrated that 84% of CO from DK3 is due to release from the composite. No cytotoxicity was observed in the cells as a result of inhibiting the cellular diffusion of the DKs and the photoproducts using a micelle. These results suggest that encapsulation of CORMs using a micelle is an effective strategy reduce cytotoxicity while providing stable transport of CO into living cells.

Nanoparticles (NPs) have also been also utilized as carriers of CORMs,[55-57] because NPs can enter cell membranes, and their surfaces can serve as chemical modification templates for introduction of coordination sites in the construction of CORMs.

Janiak *et al.* described a magnetic Fe_2O_3 NP with 9 ± 2 nm diameter functionalized with covalently anchored phenylalanine derivatives for reconstruction of the coordination sites of CORM-3 on the surface (Fig. 6d).[55] It was found that provision of a magnetic field triggers CO release from the composite with a $t_{1/2}$ of 7 ± 2 min. SiO_2 and carbon nanodiamond (ND) NPs were modified with $[Mn(CO)_3(tpm)]^+$ moieties in a Cu-catalyzed 1,3-dipolar azide-alkyne cycloaddition reaction (Fig. 6e).[56,57] The Mn carbonyl-functionalized SiO_2 and ND NPs have diameters of, 20 and 10 nm, respectively. CO is released from these composites by irradiation with 365 nm light. Although these NP-based CORMs have not been investigated in cellular assays, they might be utilized as tissue specific, time and spatially controlled CO releasing materials.

Moreover, NPs have been applied as templates in an upconversion system to achieve NIR-responsive CO release.[58] Ford and co-workers utilized a Tm and Yb-doped NaGdF$_4$ upconversion nanoparticle (UCNP) as a template for construction of CORMs.[58] When the UCNP is irradiated with NIR light, the molecule emits visible range photons which have the potential to trigger CO release. To achieve NIR-induced CO release, the UCNP and a $[Mn(bpy)(CO)_2(PPh_3)_2]^+$ complex were simultaneously encapsulated in an amphiphilic phospholipid-functionalized PEG micelle (Fig. 6f). The PEG micelles provide MnCO loading sites in the hydrophobic region, so that the MnCO moiety is in close proximity to the UCNPs to induce effective upconversion. The composite has a 16-30 nm diameter and 980 nm NIR-induced CO release was observed.

These studies demonstrate that cellular transport materials can provide coordination sites for CORMs through encapsulation and chemical modification. Encapsulation provides sustained CO release and inhibition of diffusion of CORMs.

Fig. 6. Schematic images of CORM-conjugated materials for cellular transport. The images represent (a) CORM-3-encapsulated PEG micelle,[18] (b) CORM-2-encapsulated SMA micelle,[53] (c) DKs-encapsulated Pluronic F127 micelle,[54] (d) CORM-3-modified Fe_2O_3 NP,[55] (e) Mn carbonyl-modified SiO_2 and ND NPs,[56,57] and (f) UCNP- and MnCO-encapsulated PEG micelle.[58]

3-1-2. Tissue-targeting materials

Unlike the micelle- and NP-based carriers of CORMs, dendrimers,[59] copolymers,[60] and porous materials[61-63] have been utilized as tissue-targeting scaffolds. These scaffolds are expected to accumulate passively and selectively in tumor tissues as a result of the enhanced permeability and retention effect.[60,61]

Smith *et al.*, modified dendritic scaffolds with a [MnBr(bpy)(CO)$_3$] moiety to obtain CO-releasing metallodendrimers (Fig. 7a).[59] Upon irradiation of the metallodendrimers with 410 nm light, 1.5-15.2 equiv. of CO ligands were dissociated from the composites in a $t_{1/2}$ range of 7.4-16.8 min. The $t_{1/2}$ values depend on the molecular weights of the dendritic scaffolds. It was indicated that the composites might be suitable for sustained-release of large amounts of CO (15.2 equiv. of CO per dendrimer).

Kunz and co-workers reported conjugation of a [(bpma)Mn(CO)$_3$]$^+$ moiety to 2-hydroxypropyl methacrylamide (HPMA) copolymer (Fig. 7b).[60] The $t_{1/2}$ for CO release was found to be 20 min under 365 nm light exposure. Composites with molecular weights below approximately 50 kDa did not show any cytotoxicity in HepG2 cells. Cytotoxic effects were induced when the molecular weight was increased above approximately 50 kDa. It was indicated that there are optimized sizes of the copolymer scaffolds for utilizing biological assays.

Porous materials including mesoporous silica nanoparticles (MSNPs),[61] nanoporous fibers (NFs),[62] and metal organic frameworks (MOFs)[63] have been used to incorporate CORMs. Mascharak and co-workers demonstrated that *fac*-[Mn(pqa)(CO)$_3$]ClO$_4$ can be incorporated into pores of Al-MCM-41 MSNPs (Fig. 7c).[61] The average size of the composite was found to be 58.9 ± 7.7 nm. CO is released

from the composite by irradiation with a broadband visible light source ($\lambda > 350$ nm). The utility of light-induced CO delivery by the composite has been established by promotion of relaxation of rat aorta muscle rings in tissue bath experiments. CORM-1 was incorporated into poly (L-lactide-*co*-D/L-lactide) (70:30) nanofibers by Schiller *et al.* (Fig. 7d).[62] When homogeneous fibers are constructed with a diameter of 1 μm, the composite releases 3.4 ± 0.3 μmol CO per mg of the fiber with 309 ± 51 sec of $t_{1/2}$ by irradiation with 365 nm light. The fibers provide a means of evaluating the biological effect of CO released from the composite without the effect of the photoproducts, because the photoproducts are held within the porous structures. A cytotoxic effect on mouse fibroblast 3T3 cells was induced by treatment with the composite with irradiation of 365 nm light (cytotoxicity was not observed in the dark). Metzler-Nolte and co-workers prepared MIL-88B-Fe MOFs for storage of CO gas.[63] Gas state CO was adsorbed in the MOFs under ultrahigh vacuum to produce 2.4×1.2 μm-sized spindle-shaped crystals.[63] The CO-MIL-88B-Fe MOFs release 0.36 μmol CO per 1 mg of MOFs with a $t_{1/2}$ of 38 min through degradation of the MOFs in a PBS buffer solution.

The tissue-targeting materials accumulate large quantities of CORMs within the structures by increasing the molecular size and the surface area. It is expected that these materials will achieve highly-effective targeted delivery of CO simultaneously.
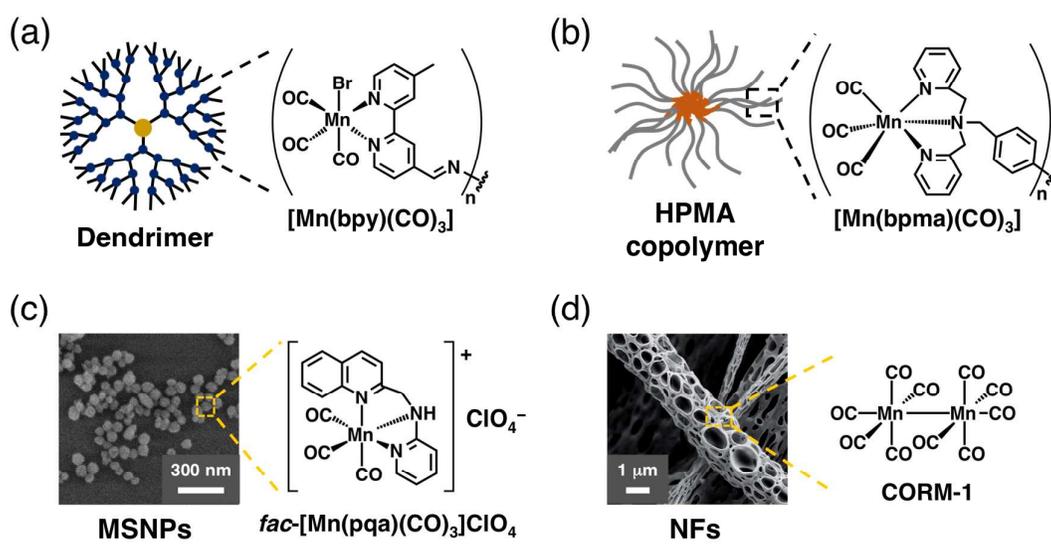
Fig. 7. Schematic images of tissue-targeting materials. (a) Dendrimer,[59] (b) HPMA copolymer,[60] (c) MSNPs,[61] and (d) NFs.[62] SEM images in (c) and (d) are reproduced from ref 61 and 62 with permission from the Royal Society of Chemistry.

3-2. Biomolecular templates

Biomolecules, such as peptides,[27,36,64-67] metabolites,[68-71] monomeric proteins,[73,74] and self-assembled supramolecular proteins[75-77] have been utilized as templates for accumulation of CORMs, because of their high biocompatibility and their available amino acid-based coordination sites for binding of CORMs through covalent and coordination bonds.

3-2-1. Peptide scaffolds

Peptide-based scaffolds have been designed to deliver CORMs, with the aim of providing effective uptake in target cells based on the specific peptide sequence.[27,36,64-67] Schatzschneider and co-workers focused on utilizing a Thr-Phe-Ser-Asp-Leu peptide which is recognized as a transactivation domain of a tumor suppressor protein p53.[64] A $[Mn(CO)_3(tpm)]^+$ moiety was conjugated to the peptide by Pd-mediated Sonogashira cross-coupling (Fig. 8a). 1.7 equiv. of CO per Mn were liberated from the composite by 365 nm light irradiation. The authors also utilized transforming growth factor (TGF) β-targeting peptide, Leu-Pro-Leu-Gly-Asn-Ser-His, as a template for coupling with CORMs.[65,66] Aldehyde-aminoxy oxime ligation was applied to conjugate a $[Mn(bpea^{CH_2C_6H_4CHO})(CO)_3]^+$ complex to the peptide (Fig. 8b).[66] The MnCO-functionalized TGF β-targeting peptide releases 1.70 ± 0.08 equiv. of CO per composite equivalent with a $t_{1/2}$ of 15.51 ± 0.52 min under 365 nm light irradiation.[66]

Stupp *et al*., synthesized self-assembled peptide nanofibers by using a C_{16} alkyl-functionalized peptide amphiphile (C_{16}-(Val)$_3$-(Ala)$_3$-(Glu)$_3$-Lys), which was conjugated to a β-sheet-forming component. The CORM-3 moiety was linked to the Lys residue at the C-terminus (Fig. 8c). CO is released from the composite with 2.16 ± 0.05

of $t_{1/2}$, which is similar to that of free CORM-3 (2.14 ± 0.17 min). This result indicates that the modified CORM-3 moiety is on the solvent-exposed site of the structure. The nanofibers have a cardioprotective effect on oxidatively stressed H9c2 rat cardiomyocytes as observed for CORM-3.

Kodanko and co-workers synthesized a $[Fe(CO)(N4Py)]^{2+}$-coupled dipeptide, Ala-Gly, as a model CO release peptide (Fig. 8d).[27] A peptide nucleic acid (PNA) was conjugated with a $[RuCl_2(bpy)(PNA)(CO)_2]$ moiety as reported by Schatzschneider and co-workers (Fig. 8e).[36] The author revealed that the composite of PNA and the Ru carbonyl moiety could release 0.3 ± 0.1 equiv. of CO with $t_{1/2}$ of 24 ± 10 min with exposure to 365 nm light.

It has been revealed that the peptides can be modified with CORMs by covalent anchoring. This modification technique will likely be applied to various cell-targeting peptides.
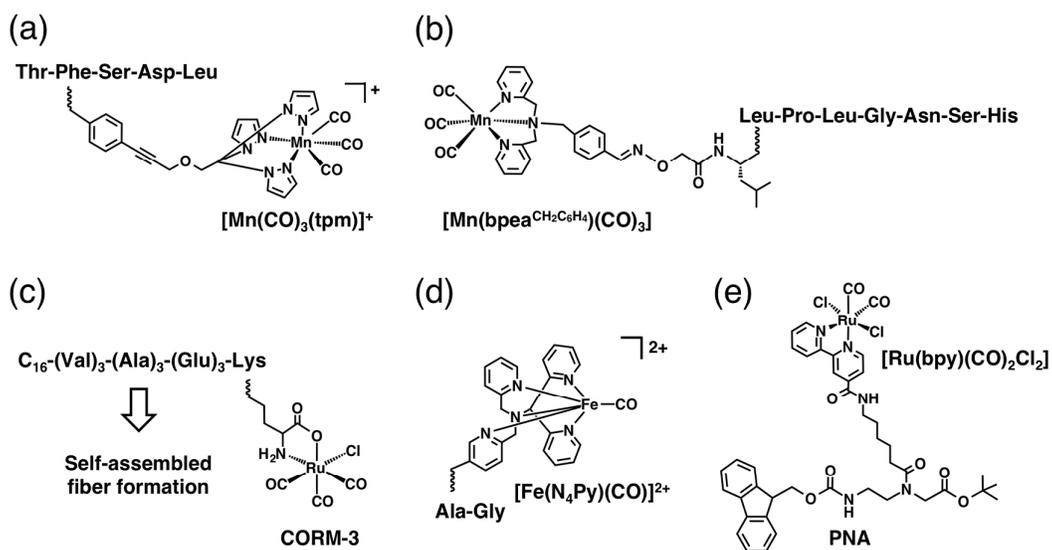
26

Fig. 8. Schematic images of CORM-conjugated peptide scaffolds. Each amino acid sequence of the peptides is represented as 3-letter characters. Modification of **(a)** $[Mn(CO)_3(tpm)]^+$ to Phe,[64] **(b)** $[Mn(bpea^{CH_2C_6H_4CHO})(CO)_3]PF_6$ to Leu,[66] **(c)** CORM-3 to Lys,[67] **(d)** $[Fe(CO)(N4Py)]^{2+}$ to Ala,[27] and **(e)** $[RuCl_2(bpy)(CO)_2]$ to a PNA scaffold.[36]

3-2-2. Metabolite scaffolds

Metabolites such as cyanocobalamin (B_{12}),[68,69] galactose,[70] 2-isocyano-2-methyl-propanoate,[71] and fumarate[72] are candidates for providing targeted delivery of CO because they can be recognized by cells and tissues.

Zobi and co-workers utilized the molecular backbone of B_{12}, which can be targeted by a cell specific vitamin transporter. The backbone of B_{12} was functionalized with $[Re(CO)_2Br_2]$[68] and $[(tacd)Mn(CO)_3]^{+}$[69] moieties to incorporate CO release units (Fig. 9a, 9b). The B_{12}-ReCO composite releases 1.0 equiv. of CO per Re, and the $t_{1/2}$ is 20 min. However, no uptake of the composite into neonatal rat cardiomyocytes was observed by atomic absorption spectroscopy (AAS).[68] To improve the uptake efficiency, the 5′-OH ribose group of B_{12} was functionalized with a $[(tacd)Mn(CO)_3]^{+}$ complex to retain the Co-coordinated cyanide ligand which can be recognized by transcobalamin, a cell specific vitamin transporter.[69] The uptake of B_{12}-MnCO into 3T3 fibroblasts was confirmed by AAS, and its localization in the nucleus and cytosol was observed by high-resolution IR spectromicroscopy. CO release of the composite was induced by irradiation with 470 nm light. It was determined that 3.0 equiv. of CO ligands are liberated per Mn equivalent. Cytoprotective effects of the released CO on the fibroblasts were confirmed under conditions of hypoxia and metabolic depletion.

Romão and co-workers synthesized a galactose-based CORM (ALF492), which consists of β-D-thiogalactopyranoside and a CORM-2 moiety (Fig. 9c), to target asialoglycoprotein receptor in the liver.[70] ALF492 releases 1.0 equiv. of CO per Ru with $t_{1/2}$ of 7.5 min. Since ALF492 has a marked affinity for the liver in mice, the compound fully protects mice from experimental cerebral malaria associated with an expression of HO-1. This is an important cytoprotective factor. The same researchers also constructed

a Mo carbonyl-coupled CORM, $[Mo(CNCMe_2CO_2H)_3(CO)_3]$ (ALF794) (Fig. 9d), which was found to accumulate in the liver of mice.[71] After intravenous injection of the ALF794 to mice, it was found that 1.2 equiv. of CO is released from the composite, as estimated using extracted liver microsomes and gas chromatography. The selective CO delivery of ALF794 reduces acetaminophen-induced severe acute liver injury in a dose-dependent manner.

Motterlini and co-workers designed hybrid CORMs (HYCOs) which activate transcription factor Nrf2 and release CO simultaneously.[72] These researchers focused on fumarate derivatives, which have been utilized in the citric acid cycle as Nrf2 activator candidates because these derivatives exert cardio-protective effects through activation of Nrf2. The fumarate derivatives coupled with the $[Co_2(CO)_6]$ moiety (HYCO-1) release 1.3 equiv. of CO with $t_{1/2}$ of 21 min (Fig. 9e). HYCO-1 induces nuclear accumulation of Nrf2 and expression of its downstream target HO-1 in murine microglial BV2 cells and murine RAW 264.7 macrophages.

The metabolite scaffolds are available for cell- and tissue-targeting delivery of CORMs because they have high selectivity for biological recognitions.
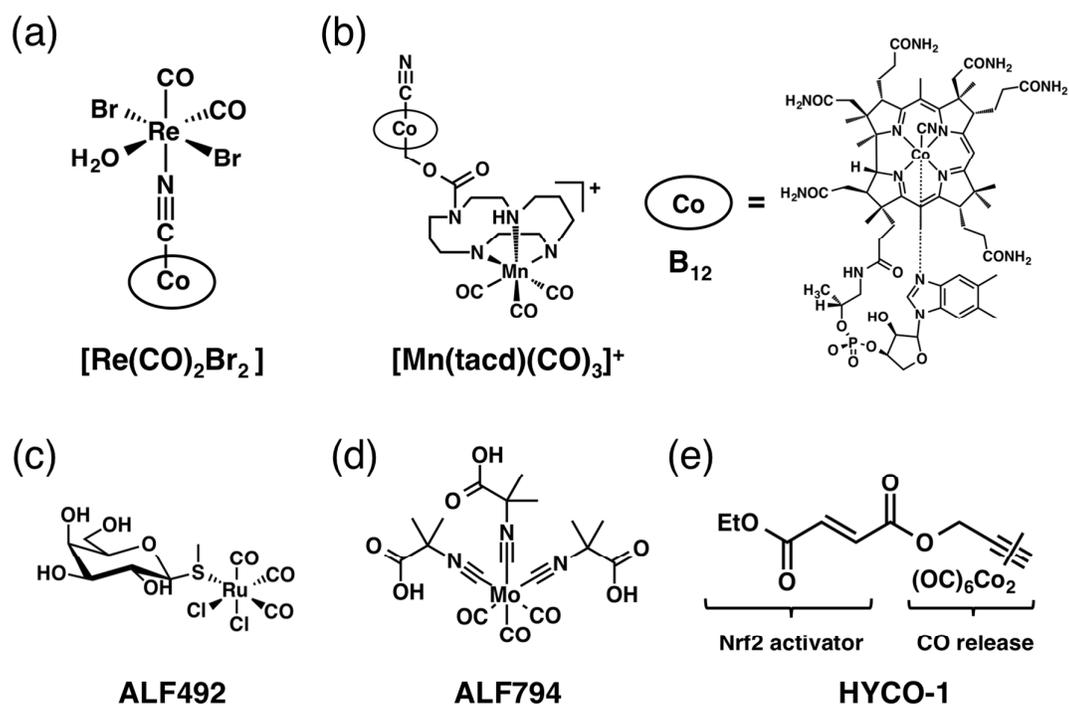
Fig. 9. Molecular scaffolds of metabolite-based CORMs. B$_{12}$-based (a) ReCO[68] and (b) MnCO,[69] (c) ALF492,[70] (d) ALF794,[71] and (e) HYCO-1.[72]

3-2-3. Protein scaffolds

In recent efforts to construct CORM carriers, protein scaffolds have received significant attention[73-77] because organometalloproteins have been used in bio-catalytic reactions[80,81] as well as intracellular delivery of metallodrugs.[82,83] Protein scaffolds including monomeric proteins[73,74] and self-assembled supramolecular proteins[75-77] can stabilize CORM moieties by coordination interactions with amino acid residues. Taking advantage of the high biocompatibility, protein scaffolds can deliver CORMs into living cells or tissues[73-75] and can accumulate on the cell surface without inducing cytotoxicity.[76,77]

Bernardes and co-workers demonstrated a strategy for designing monomeric protein scaffold-based CORMs.[73,74] Bovine serum albumin (BSA) was conjugated to CORM-2.[73] $Ru(CO)_2$ moieties were introduced into the seven His residues on the surface of the BSA (Fig. 10a). It was found that the released CO down-regulates expression levels of tumor necrosis factor (TNF)-α, interleukin (IL)-6 (proinflammatory cytokines), and IL-10 (an anti-inflammatory cytokine) in HeLa and Caco-2 cells. The composite releases CO at tumor sites in CT26 colon carcinoma-bearing mice. IL-8, which promotes neutrophil chemotaxis, can also serve as a coordination scaffold of CORM-2.[74] The CO-releasing $Ru(CO)_2$ moiety was conjugated to the His33 residue of IL-8 (Fig. 10b). The composite was found to spontaneously release CO in HeLa cells without cytotoxicity. The inherent efficacy of neutrophil chemotaxis of IL-8 was retained even after modification with the $Ru(CO)_2$ moiety.

Ueno and co-workers constructed supramolecular proteins for CORM-2 using the ferritin (Fr) cage,[75] hen-egg white lysozyme (HEWL) crystals,[76] and cypovirus

polyhedra crystals (PhCs).[77]

The Fr cage, which has an outer diameter of 12 nm, provides accumulation sites for Ru carbonyl moieties in the inner cavity (Fig. 10c).[75] The authors succeeded in modulating a coordination structure of the Ru carbonyl-modified wild-type (WT)-Fr (**Ru·Fr1**) in a rationally-designed Glu45Cys/Cys48Ala mutant. The resulting **Ru·Fr2** composite (Fig. 10d, 10e) releases 0.16 ± 0.04 equivalents of CO per Ru with $t_{1/2}$ of 35.5 ± 0.3 min. This is approximately18-fold longer than that of naked CORM-3 (2.2 ± 0.4 min). The cellular uptake ratio of Ru atoms determined for **Ru·Fr2** is approximately 4-fold higher than that of naked CORM-3. The sustained-release of CO and improvement of the uptake ratio of Ru atoms induces 10-fold activation of NF-κB in HEK293 cells relative to naked CORM-3.

Ueno and co-workers also reported on the preparation of Ru carbonyl moieties functionalized and cross-linked to a HEWL (**Ru·CL-HEWL**) crystal, as an extracellular matrix (ECM) for CO release (Fig. 10f).[76] The CO-releasing reaction was achieved by immobilization of a $[cis\text{-}Ru(CO)_2X_4]^{2-}$ unit at Asp18 in the **Ru·CL-HEWL** as confirmed by X-ray structural analysis (Fig. 10g). The **Ru·CL-HEWL** crystal releases 0.38 ± 0.02 equiv. of CO per Ru with $t_{1/2}$ of 19.4 ± 0.8 min. It is expected that the solvent channels of the CL-HEWL crystal influence the modulation of the CO release rate by restricting diffusion of trigger molecules for CO release because the $t_{1/2}$ value is about 10-fold longer than that of CORM-2 (1.9 ± 1.4 min). It was found that treatment of HEK293 cells with the **Ru·CL-HEWL** crystal induces 20% activation of NF-κB relative to the control.

A PhC was also engineered as a CO-releasing ECM by immobilizing Ru

carbonyl moieties (Fig. 10h).[77] When a hexahistidine tag (HT) was added to the C-terminus of WT-PhC, the number of Ru carbonyls accumulated in the crystal was found to increase and the amount of CO was found to increase. The HT-PhC with Ru carbonyls (**Ru·HTPhC**) releases 6.2 ± 0.9 equiv. of CO per monomer with $t_{1/2}$ of 27.7 ± 1.6 min, which is about 4-fold longer than that of naked CORM-2 (6.9 ± 2.8 min). **Ru·HTPhC** activates NF-κB 70% more than naked CORM-2.

Naturally-formed high order structures of the protein scaffolds can stabilize CORMs under biological conditions with appropriate coordination numbers and structures of CORMs modulated by amino acid replacement.
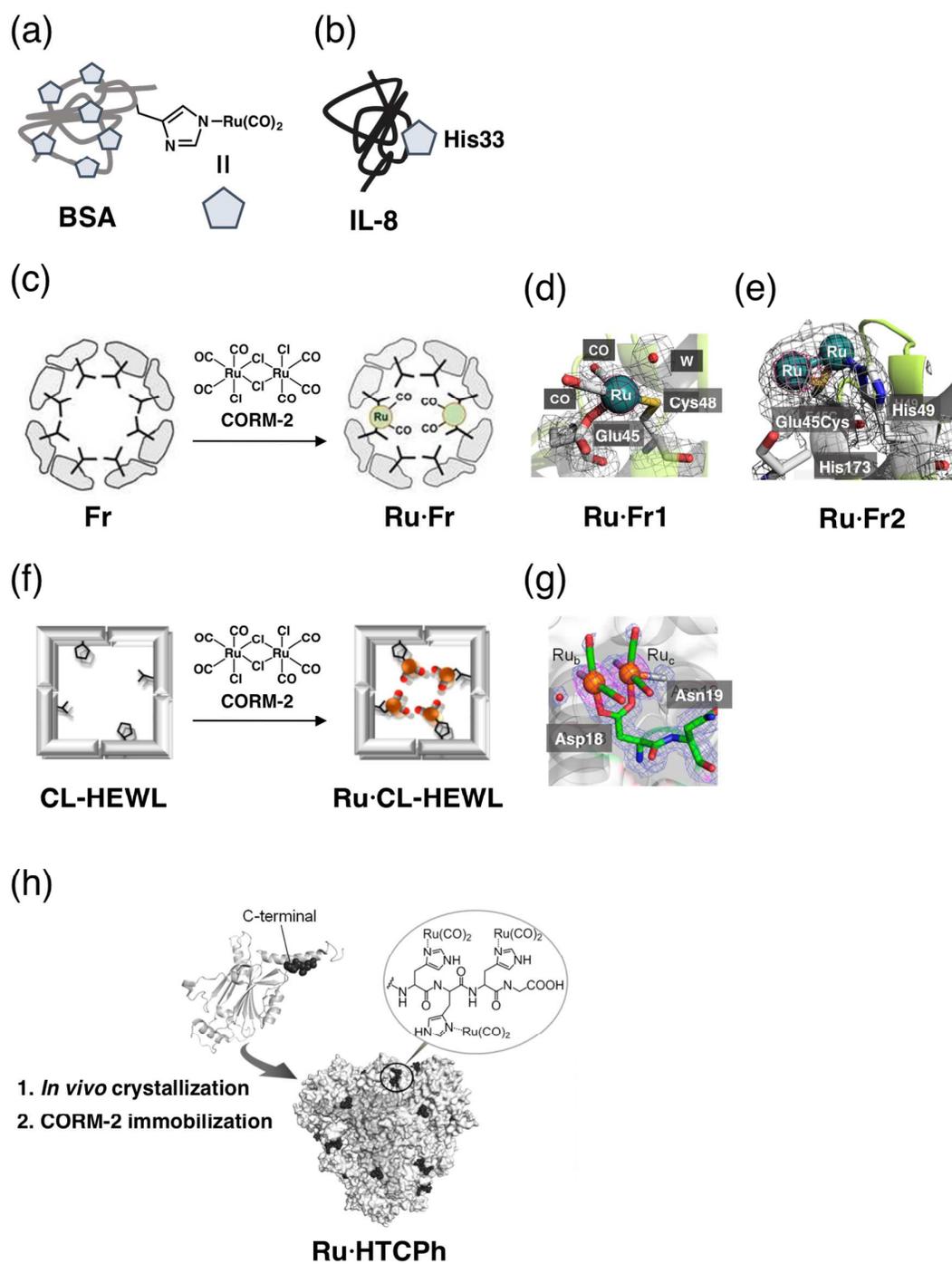
Fig. 10. Protein-based scaffolds for accumulating Ru carbonyls. The scaffolds are

(a) BSA,[73] (b) IL-8,[74] (c-e) Fr cage,[75] (f, g) HEWL crystal,[76] and (h) PhC.[77] (c)

Conjugation of Fr with CORM-2 to construct Ru·Fr. The coordination structures

of Ru complexes at the accumulation site of (d) Ru·Fr1 and (e) Ru·Fr2.[75] (f) Conjugation of CL-HEWL crystal with Ru carbonyls to construct Ru·CL-HEWL crystal. (g) The coordination structure of Ru complexes at the accumulation site of Asp18 in Ru·CL-HEWL.[76] (h) Formation of Ru·HTPhC.[77] Modified for (c)-(g) and (h) from ref 75, 76, and 77 with permission from American Chemical Society and the Chemical Society of Japan, respectively.

4. Conclusions & Perspective

This mini-review summarizes strategies for designing CORMs with molecular scaffolds to improve the process of CO delivery. Various strategies have been applied to modify the biocompatibility, CO-release rate, amount, and location. Tuning of synthetic ligands of metal carbonyls is useful to provide triggers for reactivity of CORMs using light, pH, and enzymes. Bare metal carbonyls tend to have poor solubility and stability in cellular environments, low cellular uptake efficiency. Furthermore, cellular localization is difficult to control. Incorporation of metal carbonyls into macromolecular scaffolds is a new approach to improve the biocompatibility, stability and targeting ability of CORMs *in vitro* and *in vivo*, by taking advantage of the inherent properties of the scaffolds. Macromolecular scaffolds can provide coordination sites of CORMs through chemical modification, non-covalent incorporation, and functional groups of amino acid residues. In particular, protein scaffolds are good candidates to study cellular functions of CO. Although various CORMs have been developed, there have been only a few reports investigating the correlation between the CO-releasing properties and the effects on cellular signaling pathways. In the future, the following properties of CORMs will be investigated in fundamental studies of intracellular CO and clinical applications: (1) dose and timing-controlled CO release, achievable by photo-activation; (2) organelle-targeted CO delivery with a focus on the endoplasmic reticulum, mitochondria, nucleus, and plasma membrane, where HO-1 is expressed;[10,11,13] and (3) high cellular uptake efficiency *in vitro* and *in vivo* without cytotoxicity (because uptake efficiency of the reported CORMs is low or unknown). Efforts to design CORMs with these properties are expected to reveal important information relating to intracellular CO, such as binding sites, threshold amounts, and timing of generation, for induction of

specific cellular responses. Thus, macromolecule-based CORMs are important biomaterial-based tools for studying the biological roles of CO in cellular metabolism and signal responses which ultimately govern the cell fate.

Acknowledgements

References

1   R. Motterlini and L. E. Otterbein, *Nat. Rev. Drug Discov.*, 2010, **9**, 728–743.

2   M. Kajimura, R. Fukuda, R. M. Bateman, T. Yamamoto and M. Suematsu, *Antioxid. Redox Signal.*, 2010, **13**, 157–192.

3   T. Shimizu, D. Huang, F. Yan, M. Stranava, M. Bartosova, V. Fojtíková and M. Martínková, *Chem. Rev.*, 2015, DOI: 10.1021/acs.chemrev.5b00018.

4   J. Boczkowski, J. J. Poderoso and R. Motterlini, *Trends Biochem. Sci.*, 2006, **31**, 614–621.

5   B. Wegiel, D. W. Hanto and L. E. Otterbein, *Trends in Mol. Med.*, 2013, **19**, 3–11.

6   C. C. Romão, W. A. Blättler, J. D. Seixas and G. J. L. Bernardes, *Chem. Soc. Rev.*, 2012, **41**, 3571–13.

7   S. García-Gallego and G. J. L. Bernardes, *Angew. Chem. Int. Ed.*, 2014, **53**, 9712–9721.

8   S. H. Heinemann, T. Hoshi, M. Westerhausen and A. Schiller, *Chem. Commun.*, 2014, **50**, 3644–3660.

9   R. F. Coburn, *N. Engl. J. Med.*, 1970, **283**, 512–515.

10   L. Wu and R. Wang, *Pharmacol. Rev.*, 2005, **57**, 585–630.

11   S. W. Ryter, J. Alam and A. Choi, *Physiol. Rev.*, 2006, **86**, 583–650.

12   M. D. Maines, G. M. Trakshel and R. K. Kutty, *J. Biol. Chem.*, 1986, **261**, 411–419.

13   H. P. Kim, H.-O. Pae, S. H. Back, S. W. Chung, J. M. Woo, Y. Son and H. T. Chung, *Biochem. Biophys. Res. Commun.*, 2011, **404**, 1–5.

14   H. P. Kim, X. Wang, F. Galbiati, S. W. Ryter and A. M. K. Choi, *FASEB J.*, 2004, **18**, 1080–1089.

15   R. Motterlini, J. E. Clark, R. Foresti, P. Sarathchandra, B. E. Mann and C. J. Green, *Circ. Res.*, 2002, **90**, e17–e24.

16   J. E. Clark, P. Naughton, S. Shurey, C. J. Green, T. R. Johnson, B. E. Mann, R. Foresti and R. Motterlini, *Circ. Res.*, 2003, **93**, e2–e8.

17   S. McLean, B. E. Mann and R. K. Poole, *Anal. Biochem.*, 2012, **427**, 36–40.

18   U. Hasegawa, A. J. van der Vlies, E. Simeoni, C. Wandrey and J. A. Hubbell, *J. Am. Chem. Soc.*, 2010, **132**, 18273–18280.

19   R. Motterlini, B. E. Mann and T. R. Johnson, J. E. Clark, R. Foresti and C. J. Green, *Curr. Pharm. Des.*, 2003, **9**, 2525–2539.

20   R. Motterlini, B. Haas and R. Foresti, *Med. Gas Res.*, 2012, **2**, 28.

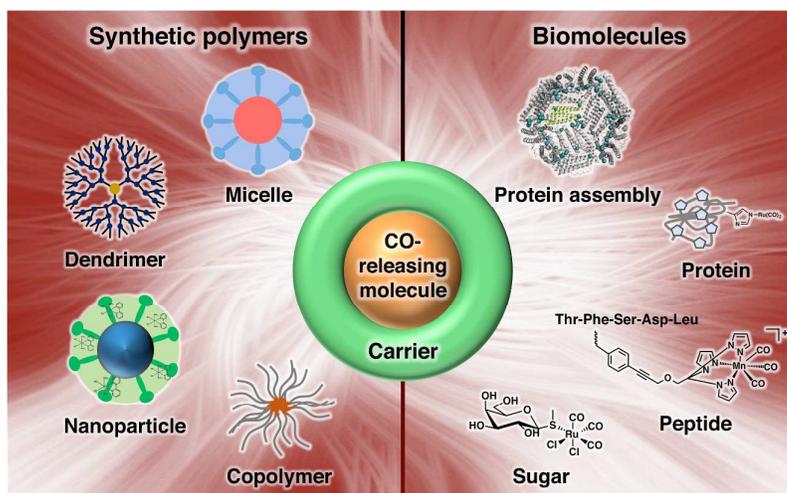21   U. Schatzschneider, *Inorg. Chim. Acta*, 2011, **374**, 19–23.

22 R. D. Rimmer, A. E. Pierri and P. C. Ford, *Coord. Chem. Rev.*, 2012, **256**, 1509–1519.

23 M. A. Gonzales and P. K. Mascharak, *J. Inorg. Biochem.*, 2014, **133**, 127–135.

24 J. Marhenke, K. Trevino and C. Works, *Coord. Chem. Rev.*, 2015, DOI: 10.1016/j.ccr.2015.02.017.

25 R. Kretschmer, G. Gessner, H. Görls, S. H. Heinemann and M. Westerhausen, *J. Inorg. Biochem.*, 2011, **105**, 6–9.

26 A. J. Atkin, I. J. S. Fairlamb, J. S. Ward and J. M. Lynam, *Organometallics*, 2012, **31**, 5894–5902.

27 C. S. Jackson, S. Schmitt, Q. P. Dou and J. J. Kodanko, *Inorg. Chem.*, 2011, **50**, 5336–5338.

28 J. S. Ward, J. M. Lynam, J. W. B. Moir, D. E. Sanin, A. P. Mountford and I. J. S. Fairlamb, *Dalton Trans.*, 2012, **41**, 10514–10517.

29 S. Pai, M. Hafftlang, G. Atongo, C. Nagel, J. Niesel, S. Botov, H.-G. Schmalz, B. Yard and U. Schatzschneider, *Dalton Trans.*, 2014, **43**, 8664–8678.

30 J. Niesel, A. Pinto, H. W. Peindy N'Dongo, K. Merz, I. Ott, R. Gust and U. Schatzschneider, *Chem. Commun.*, 2008, 1798–1800.

31 P. C. Kunz, W. Huber, A. Rojas, U. Schatzschneider and B. Spingler, *Eur. J. Inorg. Chem.*, 2009, 5358–5366.

32 M. A. Gonzalez, S. J. Carrington, N. L. Fry, J. L. Martinez and P. K. Mascharak, *Inorg. Chem.*, 2012, **51**, 11930–11940.

33 R. Mede, V. P. Lorett-Velásquez, M. Klein, H. Görls, M. Schmitt, G. Gessner, S. H. Heinemann, J. Popp and M. Westerhausen, *Dalton Trans.*, 2015, **44**, 3020–3033.

34 M. A. Gonzalez, M. A. Yim, S. Cheng, A. Moyes, A. J. Hobbs and P. K. Mascharak, *Inorg. Chem.*, 2012, **51**, 601–608.

35 S. J. Carrington, I. Chakraborty, J. M. L. Bernard and P. K. Mascharak, *ACS Med. Chem. Lett.*, 2014, **5**, 1324–1328.

36 C. Bischof, T. Joshi, A. Dimri, L. Spiccia and U. Schatzschneider, *Inorg. Chem.*, 2013, **52**, 9297–9308.

37 A. E. Pierri, A. Pallaoro, G. Wu and P. C. Ford, *J. Am. Chem. Soc.*, 2012, **134**, 18197–18200.

38 W.-Q. Zhang, A. J. Atkin, I. J. S. Fairlamb, A. C. Whitwood and J. M. Lynam, *Organometallics*, 2011, **30**, 4643–4654.

39 R. D. Rimmer, H. Richter and P. C. Ford, *Inorg. Chem.*, 2010, **49**, 1180–1185.

40 L. A. P. Antony, T. Slanina, P. Šebej, T. Šolomek and P. Klán, *Org. Lett.*, 2013, **15**, 4552–4555.

41   I. Chakraborty, S. J. Carrington and P. K. Mascharak, *Acc. Chem. Res.*, 2014, **47**, 2603–2611.

42   K. König, *J. Microsc.*, 2000, **200**, 83–104.

43   R. Motterlini, P. Sawle, J. Hammad, S. Bains, R. Alberto, R. Foresti and C. J. Green, *FASEB J.*, 2005, **19**, 284–286.

44   T. S. Pitchumony, B. Spingler, R. Motterlini and R. Alberto, *Chimia*, 2008, **62**, 277–279.

45   T. S. Pitchumony, B. Spingler, R. Motterlini and R. Alberto, *Org. Biomol. Chem.*, 2010, **8**, 4849–4854.

46   S. Romanski, B. Kraus, U. Schatzschneider, J.-M. Neudörfl, S. Amslinger and H.-G. Schmalz, *Angew. Chem. Int. Ed.*, 2011, **50**, 2392–2396.

47   S. Romanski, B. Kraus, M. Guttentag, W. Schlundt, H. Rücker, A. Adler, J.-M. Neudörfl, R. Alberto, S. Amslinger and H.-G. Schmalz, *Dalton Trans.*, 2012, **41**, 13862–13875.

48   S. Botov, E. Stamellou, S. Romanski, M. Guttentag, R. Alberto, J.-M. Neudörfl, B. Yard and H.-G. Schmalz, *Organometallics*, 2013, **32**, 3587–3594.

49   S. Romanski, H. Rücker, E. Stamellou, M. Guttentag, J.-M. Neudörfl, R. Alberto, S. Amslinger, B. Yard and H.-G. Schmalz, *Organometallics*, 2012, **31**, 5800–5809.

50   N. S. Sitnikov, Y. Li, D. Zhang, B. Yard and H.-G. Schmalz, *Angew. Chem. Int. Ed.*, 2015, DOI: 10.1002/anie.201502445.

51   S. Romanski, E. Stamellou, J. T. Jaraba, D. Storz, B. K. Krämer, M. Hafner, S. Amslinger, H. G. Schmalz and B. A. Yard, *Free Radical Biol. Med.*, 2013, **65**, 78–88.

52   E. Stamellou, D. Storz, S. Botov, E. Ntasis, J. Wedel, S. Sollazzo, B. K. Krämer, W. van Son, M. Seelen, H. G. Schmalz, A. Schmidt, M. Hafner and B. A. Yard, *Redox Biol.*, 2014, **2**, 739–748.

53   H. Yin, J. Fang, L. Liao, H. Nakamura and H. Maeda, *J. Controlled Release*, 2014, **187**, 14–21.

54   P. Peng, C. Wang, Z. Shi, V. K. Johns, L. Ma, J. Oyer, A. Copik, R. Igarashi and Y. Liao, *Org. Biomol. Chem.*, 2013, **11**, 6671–6674.

55   P. C. Kunz, H. Meyer, J. Barthel, S. Sollazzo, A. M. Schmidt and C. Janiak, *Chem. Commun.*, 2013, **49**, 4896–4898.

56   G. Dördelmann, H. Pfeiffer, A. Birkner and U. Schatzschneider, *Inorg. Chem.*, 2011, **50**, 4362–4367.

57   G. Dördelmann, T. Meinhardt, T. Sowik, A. Krueger and U. Schatzschneider, *Chem. Commun.*, 2012, **48**, 11528–11530.

58   A. E. Pierri, P.-J. Huang, J. V. Garcia, J. G. Stanfill, M. Chui, G. Wu, N. Zheng and P. C. Ford, *Chem. Commun.*, 2015, **51**, 2072–2075.

59   P. Govender, S. Pai, U. Schatzschneider and G. S. Smith, *Inorg. Chem.*, 2013, **52**, 5470–5478.

60   N. E. Brückmann, M. Wahl, G. J. Reiß, M. Kohns, W. Wätjen and P. C. Kunz, *Eur. J. Inorg. Chem.*, 2011, **2011**, 4571–4577.

61   M. A. Gonzales, H. Han, A. Moyes, A. Radinos, A. J. Hobbs, N. Coombs, S. R. J. Oliver and P. K. Mascharak, *J. Mater. Chem. B*, 2014, **2**, 2107–2113.

62   C. Bohlender, S. Gläser, M. Klein, J. Weisser, S. Thein, U. Neugebauer, J. Popp, R. Wyrwa and A. Schiller, *J. Mater. Chem. B*, 2014, **2**, 1454–1463.

63   M. Ma, H. Noei, B. Mienert, J. Niesel, E. Bill, M. Muhler, R. A. Fischer, Y. Wang, U. Schatzschneider and N. Metzler-Nolte, *Chem. Eur. J.*, 2013, **19**, 6785–6790.

64   H. Pfeiffer, A. Rojas, J. Niesel and U. Schatzschneider, *Dalton Trans.*, 2009, 4292–4298.

65   H. Pfeiffer, T. Sowik and U. Schatzschneider, *J. Organomet. Chem.*, 2013, **734**, 17–24.

66   S. Pai, K. Radacki and U. Schatzschneider, *Eur. J. Inorg. Chem.*, 2014, **2014**, 2886–2895.

67   J. B. Matson, M. J. Webber, V. K. Tamboli, B. Weber and S. I. Stupp, *Soft Matter*, 2012, **8**, 6689–6692.

68   F. Zobi, O. Blacque, R. A. Jacobs, M. C. Schaub and A. Y. Bogdanova, *Dalton Trans.*, 2012, **41**, 370–378.

69   F. Zobi, L. Quaroni, G. Santoro, T. Zlateva, O. Blacque, B. Sarafimov, M. C. Schaub and A. Y. Bogdanova, *J. Med. Chem.*, 2013, **56**, 6719–6731.

70   A. C. Pena, N. Penacho, L. Mancio-Silva, R. Neres, J. D. Seixas, A. C. Fernandes, C. C. Romão, M. M. Mota, G. J. L. Bernardes and A. Pamplona, *Antimicrob. Agents Chemother.*, 2012, **56**, 1281–1290.

71   A. R. Marques, L. Kromer, D. J. Gallo, N. Penacho, S. S. Rodrigues, J. D. Seixas, G. J. L. Bernardes, P. M. Reis, S. L. Otterbein, R. A. Ruggieri, A. S. G. Gonçalves, A. M. L. Gonçalves, M. N. D. Matos, I. Bento, L. E. Otterbein, W. A. Blättler and C. C. Romão, *Organometallics*, 2012, **31**, 5810–5822.

72   J. L. Wilson, S. Fayad Kobeissi, S. Oudir, B. Haas, B. Michel, J.-L. Dubois Randé, A. Ollivier, T. Martens, M. Rivard, R. Motterlini and R. Foresti, *Chem. Eur. J.*, 2014, **20**, 14698–14704.

73   M. Chaves-Ferreira, I. S. Albuquerque, D. Matak-Vinkovic, A. C. Coelho, S. M. Carvalho, L. M. Saraiva, C. C. Romão and G. J. L. Bernardes, *Angew. Chem. Int. Ed.*, 2014, **54**, 1172–1175.

74   I. S. Albuquerque, H. F. Jeremias, M. Chaves-Ferreira, D. Matak-Vinkovic, O. Boutureira, C. C. Romão and G. J. L. Bernardes, *Chem. Commun.*, 2015, **51**, 3993–3996.

75   K. Fujita, Y. Tanaka, T. Sho, S. Ozeki, S. Abe, T. Hikage, T. Kuchimaru, S. Kizaka-Kondoh and T. Ueno, *J. Am. Chem. Soc.*, 2014, **136**, 16902–16908.

76   H. Tabe, K. Fujita, S. Abe, M. Tsujimoto, T. Kuchimaru, S. Kizaka-Kondoh, M. Takano, S. Kitagawa and T. Ueno, *Inorg. Chem.*, 2015, **54**, 215–220.

77   H. Tabe, T. Shimoi, K. Fujita, S. Abe, H. Ijiri, M. Tsujimoto, T. Kuchimaru, S. Kizaka-Kondoh, H. Mori, S. Kitagawa and T. Ueno, *Chem. Lett.*, 2015, **44**, 342–344.

78   S. V. Zutphen and J. Reedijk, *Coord. Chem. Rev.*, 2005, **249**, 2845–2853.

79   S. M. Janib, A. S. Moses and J. A. MacKay, *Adv. Drug Deliv. Rev.*, 2010, **62**, 1052–1063.

80   M. Dürrenberger and T. R. Ward, *Curr. Opin. Chem. Biol.*, 2014, **19**, 99–106.

81   Y. Lu, N. Yeung, N. Sieracki and N. M. Marshall, *Nature*, 2009, **460**, 855–862.

82   A. MaHam, Z. Tang, H. Wu, J. Wang and Y. Lin, *Small*, 2009, **5**, 1706–1721.

83   N. M. Molino and S.-W. Wang, *Curr. Opin. Biotechnol.*, 2014, **28**, 75–82.

Table of contents

In this mini-review, current development of biomaterials as carbon monoxide-releasing molecules (CORMs) for intracellular applications is summarized and discussed.